

Article

Prediction of Uplift Capacity of Cylindrical Caissons in Anisotropic and Inhomogeneous Clays Using Multivariate Adaptive Regression Splines

Thira Jearsiripongkul¹, Van Qui Lai^{2,3,*}, Suraparb Keawsawasvong^{4,*}, Thanh Son Nguyen⁵,
Chung Nguyen Van⁶, Chanachai Thongchom⁴ and Peem Nuaklong⁴

- ¹ Department of Mechanical Engineering, Faculty of Engineering, Thammasat School of Engineering, Thammasat University, Pathumthani 12120, Thailand; jthira@engr.tu.ac.th
- ² Faculty of Civil Engineering, Ho Chi Minh City University of Technology (HCMUT), 268 Ly Thuong Kiet Street, District 10, Ho Chi Minh City 700000, Vietnam
- ³ Vietnam National University Ho Chi Minh City (VNU-HCM), Linh Trung Ward, Thu Duc District, Ho Chi Minh City 700000, Vietnam
- ⁴ Department of Civil Engineering, Faculty of Engineering, Thammasat School of Engineering, Thammasat University, Pathumthani 12120, Thailand; tchanach@engr.tu.ac.th (C.T.); npeem@engr.tu.ac.th (P.N.)
- ⁵ Faculty of Civil Engineering, Mien Trung of Civil Engineering, Tuy Hoa City 620000, Vietnam; nguyenthanson@muce.edu.vn
- ⁶ Faculty of Civil Engineering, Ho Chi Minh City University of Technology and Education, Ho Chi Minh City 71307, Vietnam; chungnv@hcmute.edu.vn
- * Correspondence: lvqui@hcmut.edu.vn (V.Q.L.); ksurapar@engr.tu.ac.th (S.K.)



Citation: Jearsiripongkul, T.; Lai, V.Q.; Keawsawasvong, S.; Nguyen, T.S.; Van, C.N.; Thongchom, C.; Nuaklong, P. Prediction of Uplift Capacity of Cylindrical Caissons in Anisotropic and Inhomogeneous Clays Using Multivariate Adaptive Regression Splines. *Sustainability* **2022**, *14*, 4456. <https://doi.org/10.3390/su14084456>

Academic Editor: Syed Minhaj Saleem Kazmi

Received: 3 March 2022

Accepted: 6 April 2022

Published: 8 April 2022

Publisher's Note: MDPI stays neutral with regard to jurisdictional claims in published maps and institutional affiliations.



Copyright: © 2022 by the authors. Licensee MDPI, Basel, Switzerland. This article is an open access article distributed under the terms and conditions of the Creative Commons Attribution (CC BY) license (<https://creativecommons.org/licenses/by/4.0/>).

Abstract: The uplift capacity factor of cylindrical suction caisson in anisotropic and inhomogeneous clays considering the adhesion factor at the interface is investigated in this paper. The finite element limit analysis based on lower bound and upper bound analyses is used for analyzing purposes. The anisotropic undrained shear model is employed to describe the anisotropic and inhomogeneous clay. The impact of these dimensionless parameters on the ratio of inhomogeneity or strength gradient ratio, the adhesion factor, the ratio of depth over diameter, and the ratio of anisotropic undrained shear strengths on the uplift resistance and the collapse mechanisms of suction caisson foundations are determined. The multivariate adaptive regression splines technique is employed to access the sensitivity of all considered dimensionless parameters on the uplift capacity factor and to propose an empirical design equation as an effective tool for predicting the uplift capacity factor. The results presented in this paper can be guidance for the preliminary design of suction caissons in anisotropic and non-homogeneous clays that are useful for engineering practitioners.

Keywords: uplift capacity; caisson; anisotropy; non-homogeneity; limit analysis; MARS

1. Introduction

Offshore geotechnical engineering is concerned with the design and construction of foundations for structures in the sea (e.g., Mortlock et al. [1]; Mahmoodian [2]). One of the favorite fixed-platform anchors is a suction caisson widely used to support floating offshore platforms, such as oil platforms, offshore drilling rigs, offshore wind turbines, and accommodation platforms to the seafloor at great depths. This suction caisson can be described as an open-bottomed tube embedded in the marine sediment. To create the negative pressure at the contact between the cap and skirt of the caisson and the soil, the water at that contact area is pumped out from the inside of the caisson. An overview of suction caissons can be found in Randolph and Gourvenec [3].

The field experiments on suction caissons were carried out by Andersen et al. [4] and Dyvik et al. [5]. The centrifuge model tests were also employed by Clukey and Morrison [6],

and Cauble [7], to study the behavior of suction caissons. By using several numerical methods, several researchers perform the numerical investigation of the response of suction caissons (e.g., Geer [8]; Bransby and Yun [9]; Gourvenec [10]; Gourvenec and Barnett [11]; Yun and Bransby [12]; Mana and Gourvenec [13]; Jin et al. [14]; Liu et al. [15]; Ukritchon et al. [16]; Keawsawasvong and Ukritchon [17]; Ukritchon and Keawsawasvong [18]). Among those researchers, Keawsawasvong and Ukritchon [17] and Ukritchon and Keawsawasvong [18] used lower bound (LB) and upper bound (UB) finite element limit analyses (FELA) (Sloan [19]), which are powerful numerical techniques to derive solutions of the uplift capacity of suction caissons. Note that the FELA technique combines the theorem of classical plasticity, the technique of numerical discretization using finite elements, and mathematical optimization. The true solutions to stability problems can be obtained by bracketing the lower bound (LB) and upper bound (UB) solutions.

Those previous works are limited to the cases of suction caissons in isotropic clays obeying the Tresca failure criterion. Ladd [20] proposed that the anisotropic properties of natural clays could have a significant effect on the capacity of foundations on anisotropic clays in which the undrained shear strengths of anisotropic clays are directionally dependent. The findings by Ladd [20] and Ladd and DeGroot [21] indicated that the strength of anisotropic clays significantly depends on three unequal undrained strengths, including the undrained strengths obtained from triaxial compression, triaxial extension, and direct simple shear. Recently, by adopting the concept of the generalized Tresca criterion by Krabbenhoft and Lyamin [22], Krabbenhoft et al. [23] proposed a novel failure criterion well-known as the anisotropic undrained shear (AUS) failure criterion for anisotropic clays. In their study, three undrained strengths were acquired from triaxial compression, triaxial extension, and direct simple shear, and they are computed in this failure criterion.

New solutions for the uplift capacity of cylindrical suction caissons in anisotropic and inhomogeneous clay with linearly increasing undrained shear strengths are presented in this paper. To derive the uplift capacity solutions, the LB and UB FELA in conjunction with the AUS failure criterion are employed. Note that several works using the FELA technique and various failure criteria for anisotropic clays have been carried out by Ukritchon and Keawsawasvong [24–28], Keawsawasvong and Ukritchon [29,30], Yodsomjai et al. [31], Keawsawasvong and Lawongkerd [32], Nguyen et al. [33], Keawsawasvong et al. [34,35], and Lai et al. [36,37] to compute the stability solutions of several geotechnical problems. In this paper, the numerical results are presented in the form of design charges and tables for practical use. The failure mechanisms of cylindrical suction caissons in anisotropic and inhomogeneous clay were also conducted in the paper to portray the essential effects of all considered parameters. Furthermore, the sensitivity of each dimensionless input parameter is investigated using the multivariate adaptive regression splines (MARS) technique. All FELA results are used as the training data in the MARS model to propose an efficient equation for engineering practitioners. It is noted that this is the first time a study has been carried out to investigate the uplift capacity of cylindrical suction caissons in anisotropic and inhomogeneous clay by using FELA, the AUS model, increasing undrained shear strengths, and the MARS model.

2. Problem Formulation

A problem definition of a cylindrical suction caisson in clay with linearly increasing anisotropic shear strength is shown in Figure 1. Due to the symmetry of the cylindrical suction caisson, only half of the domain is modelled in the FELA analysis. Note that the line of symmetry is set to be located at the left boundary of the domain. The depth and diameter of the cylindrical caisson are L and D , respectively. The caisson is assumed to be perfectly rigid and is subjected to the ultimate uplift load P . The AUS failure criterion with the associated flow rule (Krabbenhoft et al. [23]) is used as the failure criterion of anisotropic clay. Three anisotropic undrained shear strengths obtained from triaxial compression (s_{uTC}), triaxial extension (s_{uTE}), and direct simple shear (s_{uDSS}) are the input strengths of this failure criterion. In this study, the clays are assumed to be weightless (e.g., $\gamma = 0$). Note that

using the weightless is the common way to compute the pullout capacity in the undrained analysis since we only consider the part of N_c in Terzaghi's bearing capacity theory. The same approach has been applied in previous research on stability analysis under undrained conditions (e.g., references [32–35,38,39]). The adhesion factor (α) is also employed to represent the limiting shear strength at the soil–caisson interface. At the interface, the anisotropic undrained shear strengths can be defined as s_{uTCi} , s_{uTEi} , and s_{uDSSi} , which can be basically calculated from αs_{uTC} , αs_{uTE} , and αs_{uDSS} , respectively. Note that the range of α is between zero (fully smooth interface) and one (fully rough interface).

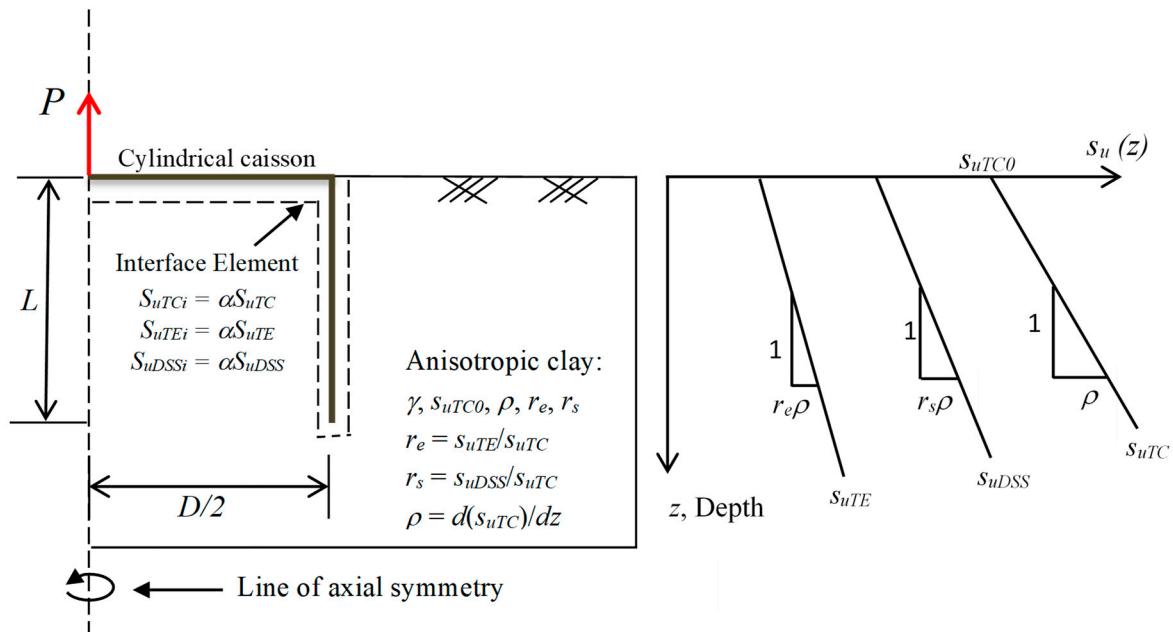


Figure 1. Problem definition of a cylindrical suction caisson in anisotropic and inhomogeneous clay.

According to the research of Krabbenhoft et al. [23] and Ladd [20], two anisotropic strength ratios for anisotropic clays can be defined as $r_e = s_{uTE}/s_{uTC}$ and $r_s = s_{uDSS}/s_{uTC}$. The harmonic mean is determined by a relationship between r_e and r_s (Krabbenhoft et al. [23]), as follows:

$$r_s = \frac{2r_e}{1 + r_e} \quad (1)$$

As seen in Equation (1), only one anisotropic strength ratio used in the parametric study is r_e since r_s is a function of r_e . Note that the range of r_e varies from 0.5 to 1. Changing in r_e can cause a change in the formation of the failure surface of the AUS failure criterion (Krabbenhoft and Lyamin [22]; Krabbenhoft et al. [23]). In addition, the cases of isotropic clays can be simulated by defining $r_e = 1$ or $s_{uTC} = s_{uTE} = s_{uDSS}$ so that the AUS failure criterion becomes the Tresca failure criterion.

An experimental investigation by Bishop [40] proved that saturated normally consolidated and lightly overconsolidated clays consist of an increment in the undrained strength, which almost linearly increases with depth. As a result, this study imposes three anisotropic undrained shear strengths (s_{uTC} , s_{uTE} , and s_{uDSS}) to be linearly increased with depth, and are expressed as:

$$s_{uTC}(z) = s_{uTC0} + \rho z \quad (2)$$

$$s_{uTE}(z) = s_{uTE0} + r_e \rho z \quad (3)$$

$$s_{uDSS}(z) = s_{uDSS0} + r_s \rho z \quad (4)$$

where s_{uTC0} , s_{uTE0} , and s_{uDSS0} denote the anisotropic undrained shear strengths at the ground surface; ρ denotes the linear strength gradient; and z denotes the depth measured from the ground surface.

By adopting the dimensionless technique, the considered parameters can be reduced so that four dimensionless input parameters are employed in this study, which can be written as a function of the uplift capacity factor as follows:

$$N = \frac{P}{As_{uTC0}} = f\left(\frac{L}{D}, \alpha, r_e, m = \frac{\rho D}{s_{uTC0}}\right) \quad (5)$$

$$A = \frac{\pi}{4}D^2 \quad (6)$$

where $N = P/As_{uTC0}$ represents the uplift capacity factor; L/D represents the ratio of depth to diameter; α represents adhesion factor at the interface between caisson and clay; m or $\rho D/s_{uTC0}$ represents the shear strength gradient ratio; and r_e represents the anisotropic strength ratio. The ranges of four dimensionless parameters in all studied cases of the paper are presented in Table 1. Considering the ranges of parameters can show the effect of the variability of soil properties in the real design (e.g., references [41,42]). It is useful for practical engineers in the initial design.

Table 1. Range of parameter.

Parameters	Input Values
L/D	0.2, 0.6, 1, 2, 5, 10
$m = \rho H/s_{uTC0}$	0, 0.2, 0.6, 1, 2, 5
α	0, 0.2, 0.4, 0.6, 0.8, 1
r_e	0.5, 0.6, 0.7, 0.8, 0.9, 1.

3. Modelling of Cylindrical Suction Caisson

The commercial software for the LB and UB FELA, namely OptumG2 [43], is used to numerically derive the uplift capacity factor of the cylindrical suction caissons in anisotropic and inhomogeneous clays with linearly increasing strengths. In OptumG2, UB elements employ six-node elements with the quadratic interpolation of unknown displacements being continuous between elements, while LB elements employ three-node elements with the linear interpolation of unknown stresses, where stress discontinuity is permitted to occur at the shared edges of adjacent triangles [44–46].

The FELA model of a cylindrical suction caisson subjected to a vertical uplift load is shown in Figure 2. In this paper, the undrained stability analyses of a spherical cavity in anisotropic clay cover a wide range of input parameters as follows: cover depth $L = 0.2$ – 10 m, $D = 1$ m, soil unit weight = 0 , $s_{uTC0} = 4$ – 20 kPa, and $r_e = 0.5$ – 1 . Note that each studied dimensionless parameter in the following analyses covers a wide range (show in Table 1), as follows: (1) $L/D = 0.2$ – 10 ; (2) $m = 0$ – 5 ; and (3) $\alpha = 0$ – 1 (4) $r_e = 0.5$ – 1 . The utilized input values of each parameter do not affect the solutions to the established dimensionless problem. The standard boundary conditions are imposed in the FELA analysis for all numerical models. The efficient technique of automatic mesh adaptivity with shear dissipation control is activated in OptumG2 in order to increase the accuracy of the computed LB and UB results. Using this technique, meshes will automatically increase in sensitive zones with high plastic-shearing strain. This study employs five adaptive steps of meshing with an initial mesh number of 5000 elements and a final mesh number of 10,000 elements. Note that the final adaptive meshes can be used as the revealed failure mechanisms of cylindrical caissons in anisotropic and inhomogeneous clay obeying the AUS failure criterion. The full-tension contact at the soil–structure interface is assumed to simulate the fully developed suction force between the cap and the skirt of the caisson and the underlying clay. The ultimate uplift load P is computed using LB and UB FELA analyses in OptumG2. The ultimate uplift load is then normalized to obtain the uplift capacity factor N according to the expression in Equation (5).

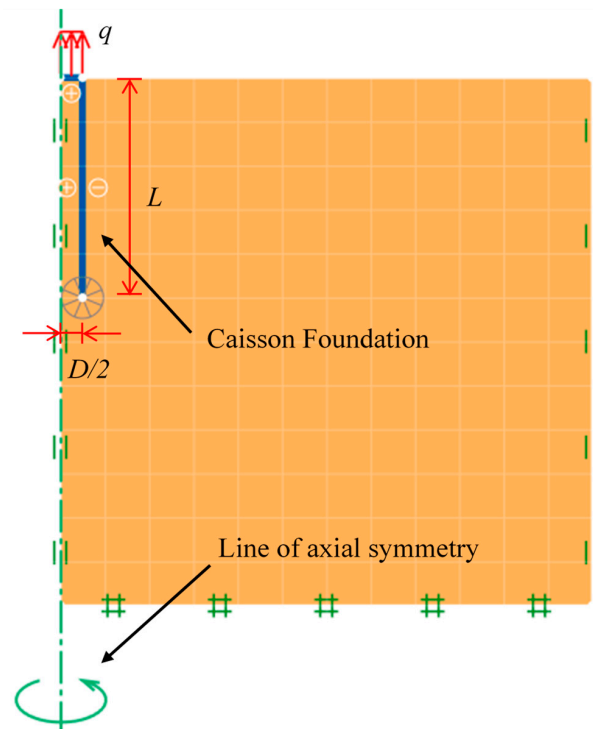


Figure 2. Numerical model of a cylindrical suction caisson in OptumG2.

4. Verification

The results of the uplift capacity factor of a cylindrical suction caisson, N , are determined from LB and UB FELA to be the average solutions, and these results are compared with previous works. The comparison is the cases of cylindrical suction caissons in homogeneous and isotropic clays, where $r_e = 1$ and $m = 0$. The obtained results are compared with the existing results: (i) the results from finite element analysis by Ukritchon et al. [16], (ii) the results from finite element limit analysis by Keawsawasvong et al. [34]. The comparison is shown in Figure 3. It can be seen that the present results are well fitted with the previous works for all cases of different values of the adhesion factor ($\alpha = 0, 0.2, 0.4, 0.6, 0.8,$ and 1).

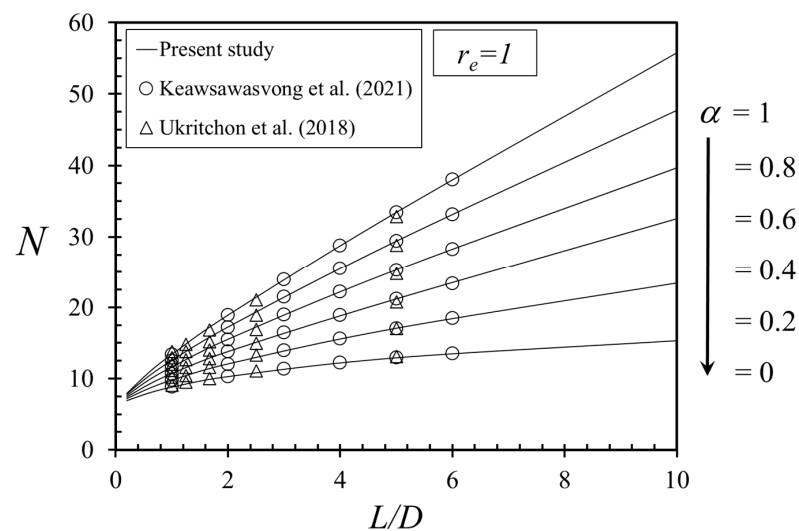


Figure 3. Comparison of the present study and those available from the literature for the cases of isotropic and homogenous clays ($r_e = 1, m = 0$).

5. Numerical Results and Discussion

In this paper, all results of the uplift bearing factor N obtained from the average values between LB and UB FELA are prepared in Tables 2–4. Figure 4 shows the variation of the uplift capacity factor N by changing the ratio of depth over diameter L/D for the cases of $\alpha = 0.7$ with $m = (0, 0.6, 1, 5)$. As a result, the nonlinear relationship between the uplift capacity factor N and the ratio of depth over diameter L/D can be observed for all cases of m and r_e . An increase in L/D yields a nonlinear increase in N . It is due to the fact that increasing the size of the caisson can directly increase the uplift capacity. Furthermore, as seen in Figure 4a, the nonlinear relationship is convex while the others show the concave relationships in Figure 4b–d. The rate of the increase (or gradient of line) of N in Figure 4b–d is changed to be higher when the value of L/D is approximately larger than five. Additionally, an increase in the value of r_e and m can produce an increase in N . The impacts of L/D on the failure patterns of the final adaptive meshes of suction caisson in anisotropic and inhomogeneous clays for the cases of $r_e = 0.7$, $\alpha = 1$, and $m = 5$ with $L/D = (1, 2, 5, 10)$ are shown in Figure 5a–d, respectively. The shear dissipation contours of the suction caisson for the same cases are shown in Figure 6a–d. It can be seen that the refined mesh contains a large number of elements in the shear failure zones. As the values of L/D increase, the sizes of the failure patterns increase in both horizontal and vertical directions. The failure zones start from the bottom of the caisson and go up to the ground surface. This is the typical failure type of an uplifting foundation. Based on these failure patterns, it can be concluded that an increase in the size of the failure pattern cooperates with an increase in L/D .

Table 2. Results obtained from the present analysis for the cases of $m = 0$ and $m = 0.2$.

α	L/D	$m = 0$						$m = 2$					
		r_e						r_e					
		0.5	0.6	0.7	0.8	0.9	1	0.5	0.6	0.7	0.8	0.9	1
0.0	0.2	4.03	4.68	5.29	5.86	6.41	6.93	4.35	5.05	5.70	6.32	6.90	7.46
	0.6	4.66	5.40	6.11	6.77	7.41	8.02	5.38	6.24	7.05	7.81	8.54	9.24
	1	5.10	5.93	6.71	7.44	8.14	8.82	6.27	7.28	8.22	9.12	9.97	10.80
	2	5.92	6.89	7.80	8.67	9.50	10.31	8.31	9.66	10.93	12.14	13.29	14.41
	5	7.29	8.51	9.69	10.81	11.90	12.96	14.00	16.32	18.54	20.65	22.72	24.72
	10	8.42	9.91	11.35	12.73	14.06	15.36	23.60	27.61	31.45	35.13	38.78	42.33
0.2	0.2	4.17	4.84	5.47	6.07	6.63	7.17	4.50	5.22	5.90	6.53	7.14	7.71
	0.6	5.04	5.84	6.59	7.30	7.97	8.62	5.80	6.71	7.57	8.38	9.15	9.89
	1	5.71	6.62	7.47	8.26	9.03	9.76	6.95	8.05	9.08	10.05	10.97	11.85
	2	7.06	8.17	9.22	10.21	11.15	12.05	9.71	11.24	12.67	14.02	15.31	16.54
	5	10.02	11.59	13.07	14.47	15.80	17.08	18.16	21.00	23.70	26.23	28.68	31.02
	10	13.80	15.97	18.01	19.92	21.74	23.47	34.48	39.86	44.91	49.67	54.30	58.73
0.4	0.2	4.31	5.00	5.65	6.26	6.84	7.40	4.65	5.39	6.09	6.74	7.36	7.96
	0.6	5.42	6.27	7.07	7.82	8.53	9.21	6.21	7.18	8.09	8.94	9.76	10.53
	1	6.31	7.30	8.21	9.08	9.90	10.69	7.62	8.81	9.92	10.96	11.95	12.90
	2	8.19	9.45	10.63	11.73	12.78	13.79	11.09	12.80	14.39	15.88	17.31	18.67
	5	12.74	14.66	16.44	18.11	19.69	21.19	22.29	25.67	28.82	31.77	34.60	37.28
	10	19.17	22.02	24.65	27.10	29.40	31.56	45.34	52.07	58.34	64.18	69.78	75.07

Table 2. Cont.

0.6	0.2	4.44	5.15	5.81	6.44	7.04	7.62	4.78	5.54	6.26	6.93	7.57	8.19
	0.6	5.79	6.69	7.53	8.32	9.08	9.84	6.62	7.64	8.60	9.50	10.35	11.16
	1	6.90	7.96	8.95	9.88	10.76	11.60	8.29	9.56	10.75	11.86	12.92	13.92
	2	9.32	10.72	12.03	13.25	14.41	15.50	12.46	14.34	16.09	17.73	19.29	20.77
	5	15.46	17.72	19.80	21.75	23.57	25.29	26.41	30.31	33.92	37.29	40.49	43.51
	10	24.53	28.06	31.29	34.27	37.06	39.65	56.16	64.26	71.74	78.65	85.21	91.38
0.8	0.2	4.55	5.28	5.96	6.60	7.22	7.81	4.90	5.68	6.41	7.10	7.76	8.39
	0.6	6.16	7.11	8.00	8.83	9.62	10.37	7.01	8.09	9.10	10.04	10.94	11.79
	1	7.49	8.63	9.69	10.68	11.62	12.51	8.94	10.31	11.57	12.75	13.87	14.94
	2	10.44	11.98	13.42	14.76	16.02	17.21	13.82	15.88	17.79	19.57	21.26	22.85
	5	18.17	20.77	23.16	25.37	27.44	29.39	30.51	34.93	39.01	42.79	46.36	49.73
	10	29.89	34.09	37.92	41.44	44.70	47.73	66.96	76.43	85.11	93.09	100.65	107.65
1.0	0.2	4.60	5.34	6.04	6.70	7.33	7.93	4.95	5.75	6.49	7.20	7.87	8.52
	0.6	6.46	7.34	8.42	9.30	10.05	10.93	7.33	8.49	9.56	10.55	11.50	12.39
	1	7.99	9.24	10.39	11.45	12.45	13.40	9.53	10.99	12.35	13.62	14.75	15.94
	2	11.45	13.21	14.79	16.25	17.62	18.91	15.08	17.36	19.45	21.38	23.19	24.90
	5	20.82	23.77	26.49	28.98	31.29	33.43	34.49	39.49	44.06	48.25	52.20	55.88
	10	35.19	40.08	44.52	48.56	52.30	55.75	77.49	88.42	98.40	107.50	115.90	123.80

Table 3. Results obtained from the present analysis for the cases of $m = 0.6$ and $m = 1$.

α	L/D	$m = 0.6$						$m = 1$					
		r_e						r_e					
		0.5	0.6	0.7	0.8	0.9	1	0.5	0.6	0.7	0.8	0.9	1
0.0	0.2	4.95	5.74	6.48	7.17	7.83	8.46	5.52	6.40	7.22	7.98	8.71	9.41
	0.6	6.77	7.84	8.86	9.81	10.72	11.58	8.12	9.41	10.62	11.76	12.84	13.87
	1	8.52	9.89	11.16	12.37	13.52	14.62	10.73	12.44	14.05	15.56	17.00	18.38
	2	12.96	15.05	17.02	18.88	20.66	22.38	17.56	20.39	23.04	25.55	27.95	30.27
	5	27.19	31.65	35.91	39.95	43.92	47.76	40.32	46.91	53.20	59.17	65.01	70.68
	10	53.48	62.47	71.11	79.37	87.57	95.52	83.31	97.29	110.70	123.55	136.25	148.65
0.2	0.2	5.12	5.93	6.69	7.41	8.08	8.73	5.70	6.61	7.45	8.24	8.99	9.70
	0.6	7.25	8.39	9.46	10.47	11.42	12.34	8.66	10.02	11.30	12.50	13.63	14.72
	1	9.35	10.82	12.20	13.49	14.73	15.91	11.70	13.54	15.26	16.88	18.41	19.89
	2	14.86	17.19	19.39	21.44	23.41	25.30	19.96	23.09	26.02	28.79	31.43	33.96
	5	34.16	39.53	44.59	49.35	53.96	58.38	50.12	57.99	65.39	72.39	79.16	85.64
	10	75.32	87.07	98.16	108.60	118.80	128.50	116.10	134.20	151.30	167.45	183.15	198.15
0.4	0.2	5.28	6.12	6.90	7.63	8.33	9.00	5.88	6.81	7.67	8.48	9.25	9.98
	0.6	7.72	8.93	10.05	11.11	12.12	13.08	9.19	10.62	11.96	13.22	14.41	15.55
	1	10.16	11.74	13.21	14.60	15.92	17.17	12.65	14.62	16.45	18.17	19.81	21.37
	2	16.74	19.31	21.72	23.97	26.13	28.18	22.32	25.76	28.97	31.99	34.87	37.61
	5	41.12	47.37	53.21	58.68	63.94	68.94	59.89	68.99	77.51	85.50	93.16	100.50
	10	97.07	111.60	125.15	137.70	149.90	161.40	148.80	171.10	191.80	211.25	229.85	247.55

Table 3. *Cont.*

0.6	0.2	5.43	6.29	7.09	7.85	8.56	9.25	6.04	6.99	7.88	8.71	9.50	10.26
	0.6	8.18	9.45	10.63	11.74	12.80	13.80	9.71	11.21	12.61	13.93	15.17	16.36
	1	10.96	12.65	14.22	15.69	17.09	18.41	13.59	15.68	17.62	19.44	21.17	22.82
	2	18.59	21.41	24.03	26.48	28.82	31.04	24.67	28.40	31.89	35.15	38.25	41.21
	5	48.02	55.16	61.78	67.96	73.85	79.42	69.59	79.95	89.57	98.53	107.10	115.25
	10	118.80	136.10	152.00	166.80	180.90	194.10	181.40	207.80	232.20	254.85	276.40	296.75
0.8	0.2	5.55	6.43	7.27	8.03	8.77	9.48	6.17	7.15	8.06	8.91	9.73	10.51
	0.6	8.64	9.96	11.21	12.36	13.46	14.51	10.22	11.79	13.25	14.62	15.92	17.16
	1	11.75	13.54	15.21	16.76	18.24	19.64	14.51	16.72	18.78	20.70	22.52	24.26
	2	20.42	23.48	26.32	28.97	31.48	33.86	26.97	31.02	34.77	38.28	41.61	44.77
	5	54.91	62.92	70.32	77.19	83.72	89.87	79.26	90.84	101.55	111.50	120.95	129.90
	10	140.50	160.50	178.85	195.80	211.80	226.80	213.90	244.45	272.50	298.40	322.85	345.80
1.0	0.2	5.61	6.50	7.34	8.13	8.89	9.44	6.23	7.22	8.14	9.02	9.85	10.66
	0.6	9.01	10.41	11.73	12.95	14.10	15.11	10.63	12.29	13.84	15.28	16.64	17.94
	1	12.45	14.38	16.18	17.80	19.36	20.84	15.32	17.68	19.87	21.92	23.84	25.67
	2	22.12	25.46	28.56	31.41	34.10	36.65	29.11	33.53	37.59	41.36	44.92	48.28
	5	61.51	70.54	78.78	86.36	93.52	100.20	88.42	101.45	113.45	124.40	134.70	144.45
	10	161.55	184.35	205.50	224.60	242.55	259.25	245.35	280.35	312.55	341.70	369.00	394.60

Table 4. Results obtained from the present analysis for the cases of $m = 2$ and $m = 5$.

α	L/D	$m = 2$						$m = 5$					
		r_e						r_e					
		0.5	0.6	0.7	0.8	0.9	1	0.5	0.6	0.7	0.8	0.9	1
0.0	0.2	6.88	7.96	8.97	9.91	10.81	11.66	10.71	12.39	13.93	15.37	16.72	18.00
	0.6	11.44	13.25	14.94	16.54	18.04	19.49	21.23	24.59	27.71	30.64	33.43	36.08
	1	16.19	18.76	21.18	23.45	25.60	27.67	32.44	37.58	42.40	46.92	51.23	55.35
	2	29.00	33.64	38.02	42.14	46.10	49.90	63.18	73.31	82.80	91.76	100.35	108.60
	5	73.07	84.99	96.34	107.15	117.60	127.90	171.30	199.20	225.70	250.90	275.50	299.40
	10	157.80	184.25	209.60	233.85	257.90	281.25	381.25	445.10	506.25	564.80	622.80	679.00
0.2	0.2	7.09	8.20	9.24	10.21	11.12	12.00	11.00	12.71	14.29	15.77	17.15	18.46
	0.6	12.13	14.03	15.81	17.48	19.06	20.57	22.36	25.86	29.12	32.18	35.08	37.85
	1	17.52	20.26	22.83	25.25	27.54	29.74	34.81	40.27	45.37	50.16	54.70	59.07
	2	32.64	37.75	42.56	47.07	51.39	55.53	70.53	81.64	92.01	101.75	111.10	120.00
	5	89.98	104.10	117.40	129.90	142.00	153.70	209.35	242.20	273.15	302.30	330.50	357.60
	10	218.05	252.10	284.20	314.55	344.00	372.25	523.80	605.60	682.80	755.65	826.50	894.25
0.4	0.2	7.29	8.43	9.49	10.49	11.43	12.32	11.28	13.02	14.64	16.15	17.56	18.91
	0.6	12.79	14.79	16.65	18.39	20.04	21.62	23.45	27.09	30.49	33.66	36.68	39.56
	1	18.80	21.73	24.46	27.01	29.44	31.75	37.14	42.90	48.27	53.32	58.11	62.69
	2	36.23	41.81	47.03	51.92	56.60	61.06	77.77	89.82	101.05	111.55	121.60	131.20
	5	106.75	123.00	138.20	152.45	166.20	179.25	247.20	284.95	320.20	353.20	385.00	415.20
	10	277.95	319.70	358.60	394.90	429.75	462.90	665.50	765.55	858.60	945.55	1029.50	1109.00

Table 4. Cont.

0.6	0.2	7.48	8.65	9.74	10.76	11.72	12.65	11.54	13.33	14.98	16.52	17.97	19.35
	0.6	13.45	15.53	17.47	19.29	21.01	22.65	24.50	28.29	31.82	35.12	38.25	41.23
	1	20.08	23.17	26.05	28.74	31.30	33.74	39.42	45.47	51.12	56.42	61.45	66.24
	2	39.76	45.82	51.45	56.72	61.75	66.53	84.95	97.90	110.00	121.30	132.00	142.30
	5	123.45	141.80	158.95	174.85	190.15	204.55	284.90	327.35	366.90	403.85	439.15	472.55
	10	337.90	387.10	432.70	475.00	515.25	553.25	807.15	924.95	1034.00	1135.00	1231.50	1322.50
0.8	0.2	7.64	8.83	9.95	10.99	11.99	12.94	11.76	13.59	15.27	16.85	18.33	19.75
	0.6	14.09	16.26	18.27	20.16	21.96	23.66	25.54	29.46	33.11	36.53	39.77	42.86
	1	21.32	24.59	27.61	30.44	33.13	35.69	41.64	48.00	53.92	59.46	64.73	69.73
	2	43.25	49.77	55.82	61.47	66.84	71.93	91.99	105.90	118.80	130.85	142.30	153.20
	5	140.05	160.55	179.55	197.20	213.95	229.85	322.30	369.65	413.45	454.15	492.90	529.55
	10	397.60	454.30	506.60	554.80	600.45	643.30	948.35	1084.00	1209.00	1324.00	1433.00	1535.50
1.0	0.2	7.72	8.92	10.05	11.12	12.13	13.10	11.87	13.69	15.41	17.02	18.54	20.00
	0.6	14.61	16.89	19.01	20.99	22.86	24.64	26.35	30.48	34.30	37.85	41.24	44.46
	1	22.36	25.88	29.09	32.10	34.92	37.60	43.55	50.29	56.56	62.18	67.91	73.15
	2	46.48	53.56	60.10	66.13	71.83	77.26	98.40	113.60	127.40	140.25	152.40	163.95
	5	156.05	178.70	200.00	219.35	237.70	254.85	357.45	410.40	459.45	504.05	546.25	586.00
	10	454.80	520.35	580.00	634.25	685.20	732.85	1084.50	1240.00	1382.50	1512.00	1633.50	1747.50

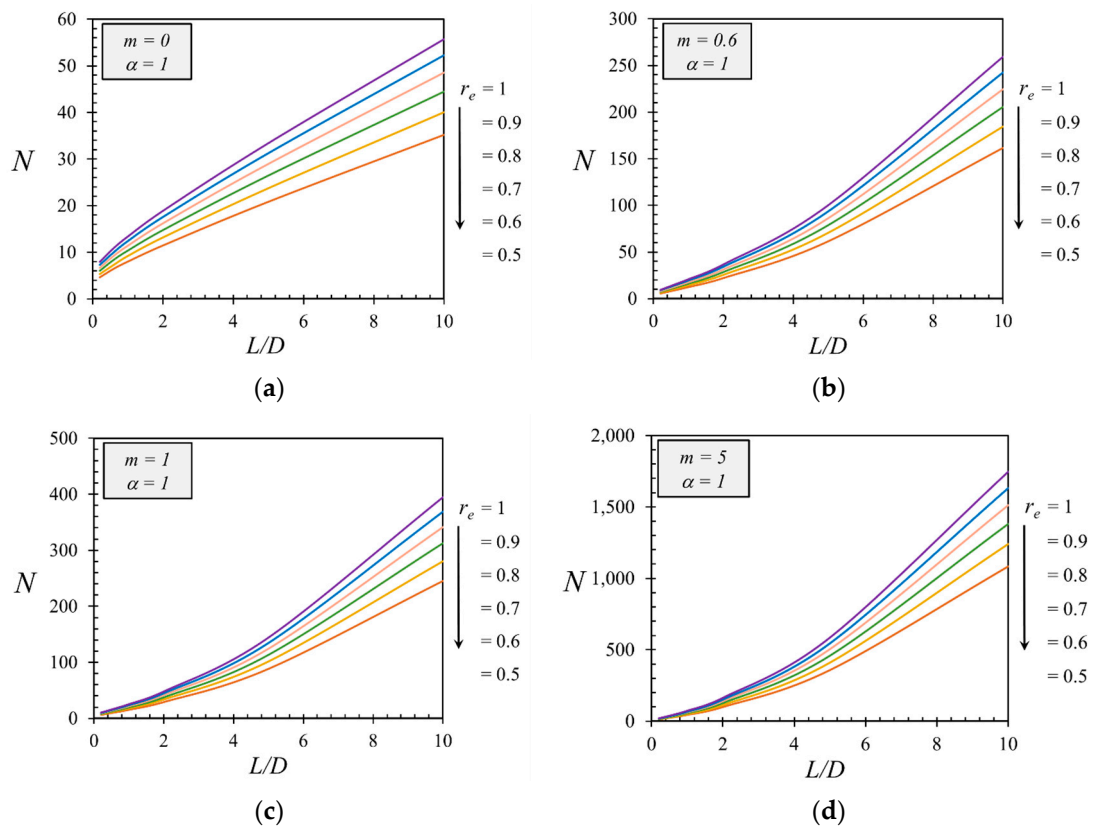


Figure 4. Impact of L/D on the uplift capacity factor N for the cases of $\alpha = 1$: (a) $m = 0$, (b) $m = 0.6$, (c) $m = 1$, (d) $m = 5$.

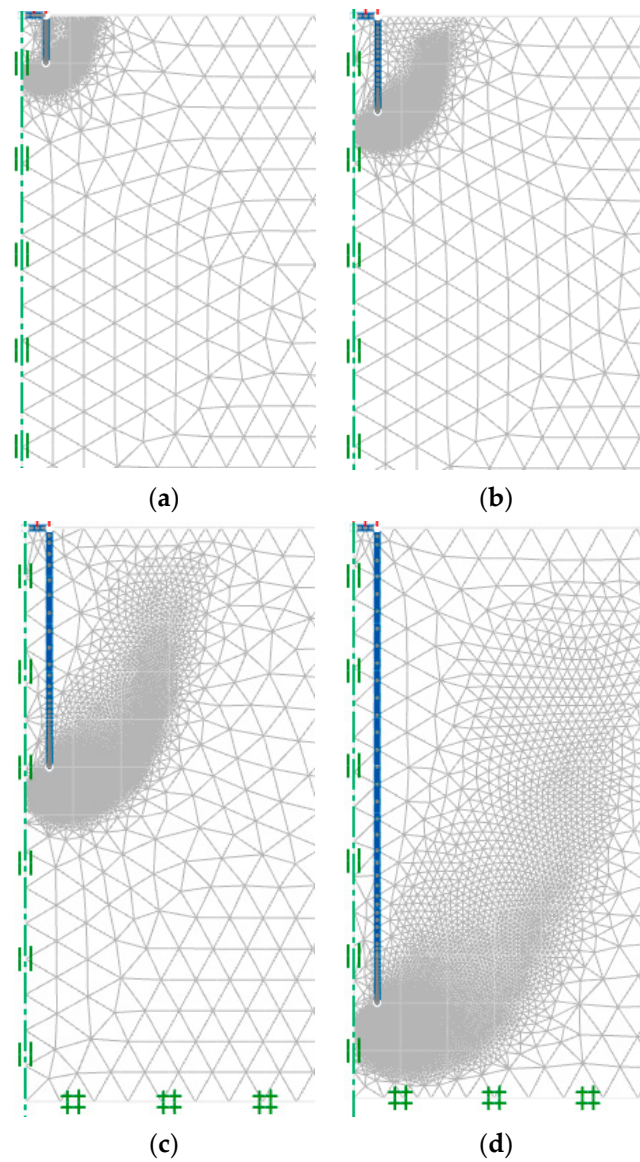


Figure 5. Failure patterns of cylindrical suction caissons in anisotropic and inhomogeneous clays for different values of L/D with $r_e = 0.7$, $\alpha = 1$, $m = 5$: (a) $L/D = 1$, (b) $L/D = 2$, (c) $L/D = 5$, (d) $L/D = 10$.

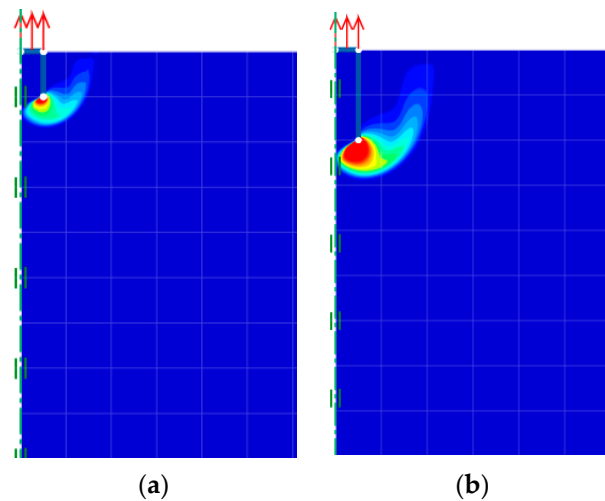


Figure 6. Cont.

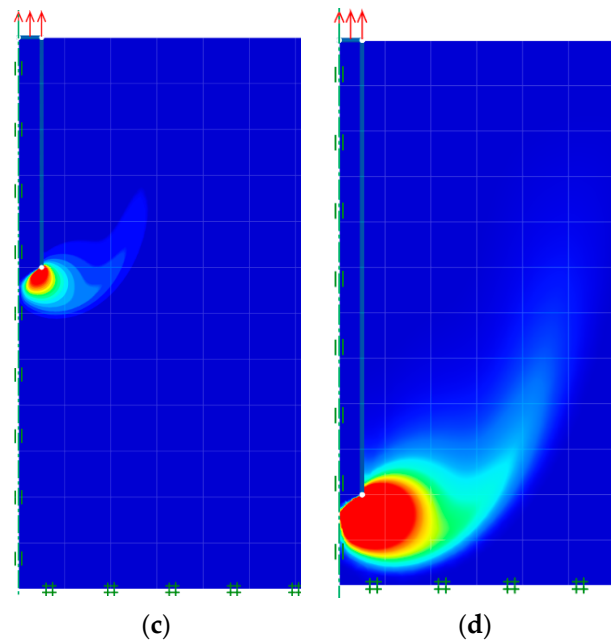


Figure 6. Comparison of shear dissipations of the cylindrical suction caissons for different values of L/D with $r_e = 0.7$, $\alpha = 1$, $m = 5$: (a) $L/D = 1$, (b) $L/D = 2$, (c) $L/D = 5$, (d) $L/D = 10$.

The effects of the shear strength gradient ratio m on the uplift bearing factor N for the cases $r_e = 0.5$ with different values of α and L/D are depicted in Figure 7. Shown in Figure 7a–d are cases of $L/D = (0.2, 0.6, 2, 5)$, respectively. A linear relationship between N and m can be observed for all cases of α and L/D . An increase in m causes a linear increase in N . This is because the caissons can obtain a more mobilized resistance due to an increase in the undrained shear strength of the soil with depth. Note that a larger value of α produces a larger value of N . In addition, together with the growth of L/D , the gradient of the N and m relationship becomes greater owing to the increase of α . The comparison of four potential failure patterns (shear dissipation contour) is described in Figure 8 for various values of $m = (0, 1, 2, 5)$. This comparison is based on the cases of $r_e = 0.9$, $L/D = 5$, and $\alpha = 1$. The results show that the failure zone increases as m increases. This finding is compatible with the results showing an increase of N due to an increase of m .

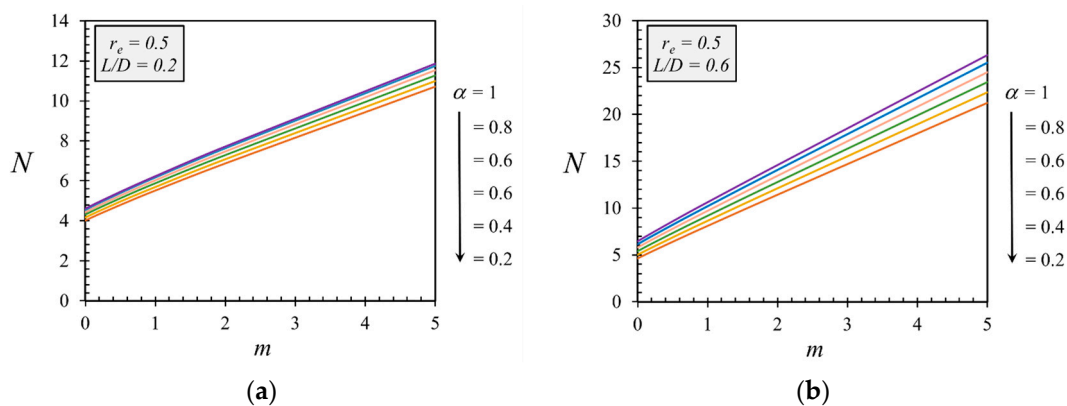


Figure 7. Cont.

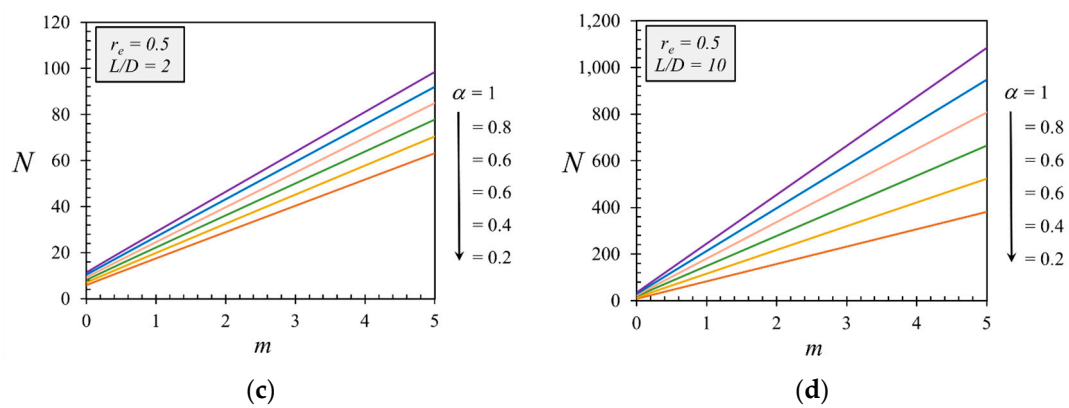


Figure 7. Impact of m on the uplift capacity factor N for the cases of $r_e = 0.5$: (a) $L/D = 0.2$; (b) $L/D = 0.6$; (c) $L/D = 2$, (d) $L/D = 5$.

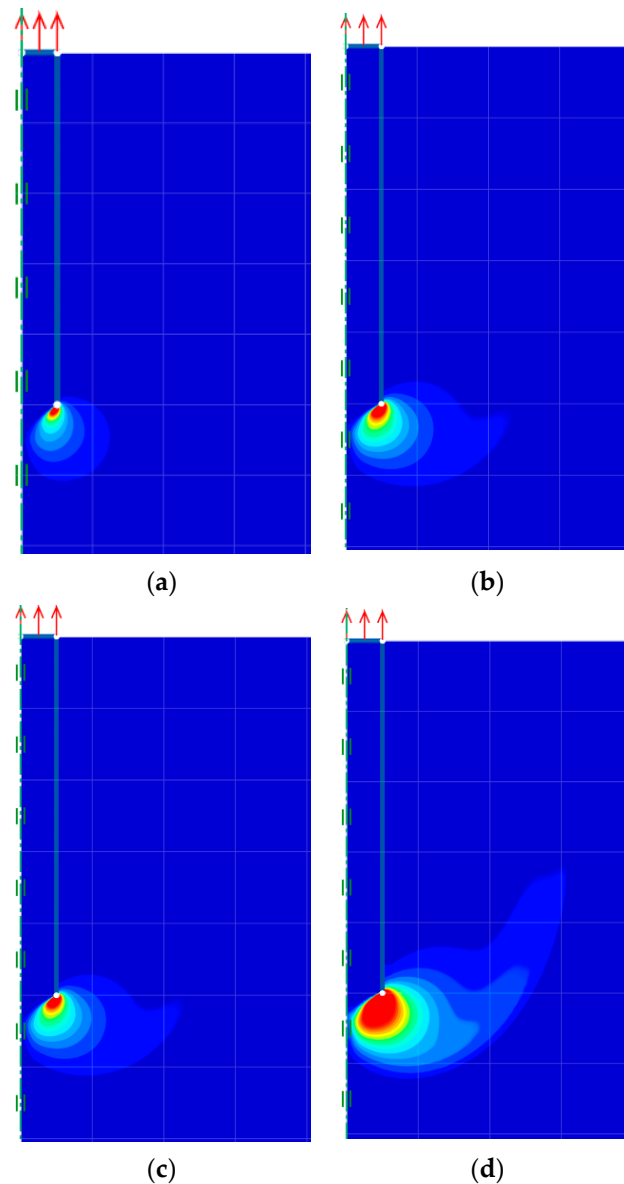


Figure 8. Comparison of shear dissipations of the cylindrical suction caissons for different values of m with $r_e = 0.9$, $L/D = 5$, $\alpha = 1$: (a) $m = 0$, (b) $m = 1$, (c) $m = 2$, (d) $m = 5$.

Figures 9 and 10 show the impacts of the adhesion factor of α on the uplift capacity factor of N and the failure patterns, respectively. As shown in Figure 9, a linear relationship between N and α is observed for all cases of $m = 1$ with various values of L/D and r_e . The value of N is not much changed by increasing α for cases of $L/D = 0.2, 0.6, 1, 2$, except for cases of $L/D = 5, 10$. This finding shows that the influence of L/D seems to be stronger than the influence of α . In Figure 10, the effect of α on the failure patterns is investigated through four cases of $\alpha = (0.2, 0.4, 0.8, 1)$ in which the other parameters are fixed as $r_e = 0.7$, $L/D = 2$, and $m = 2$. It is found that the variation of α does not significantly influence the change in failure patterns.

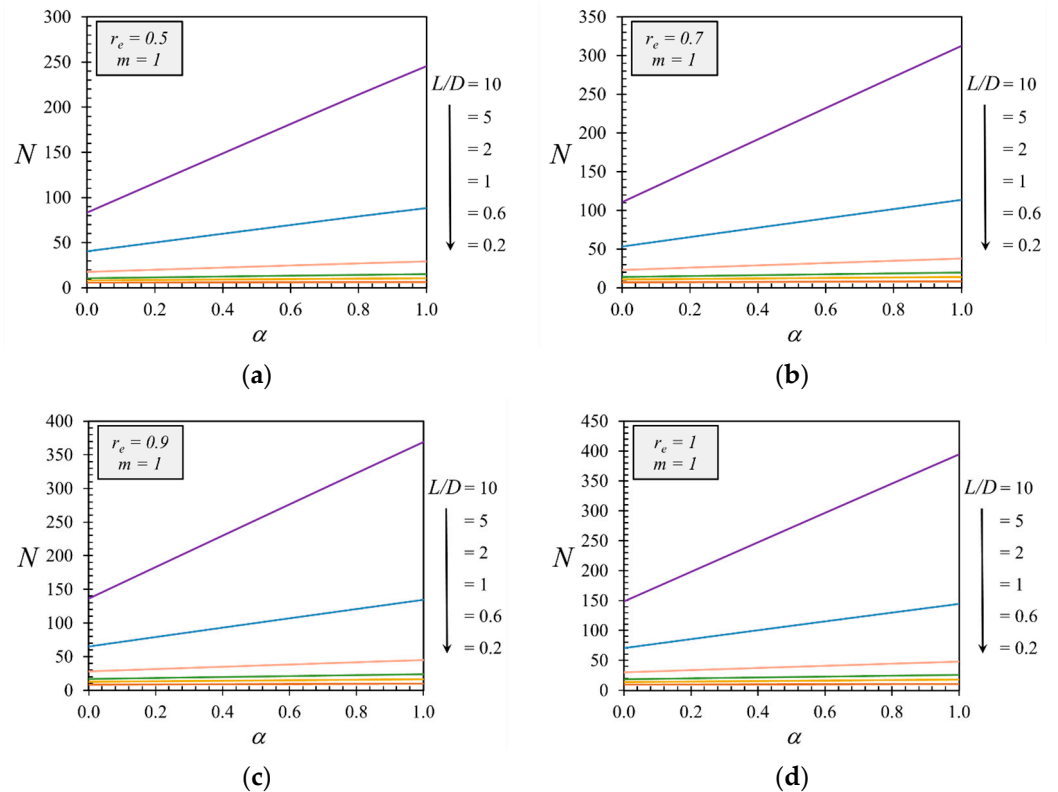


Figure 9. Impact of α on the uplift capacity factor N for the cases of $m = 1$: (a) $r_e = 0.5$, (b) $r_e = 0.7$ (c) $r_e = 0.9$, (d) $r_e = 1$.

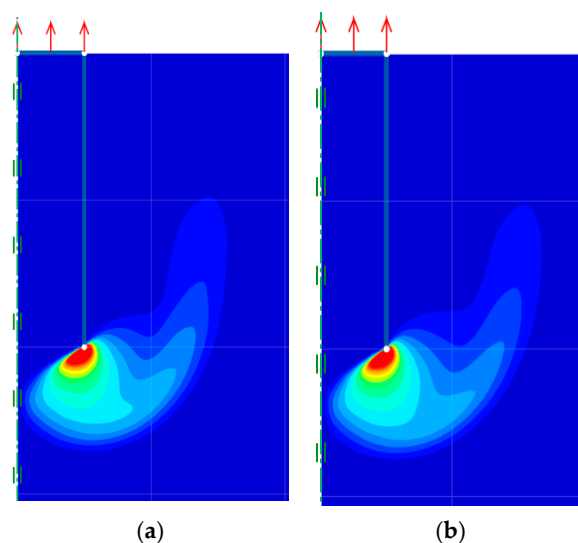


Figure 10. Cont.

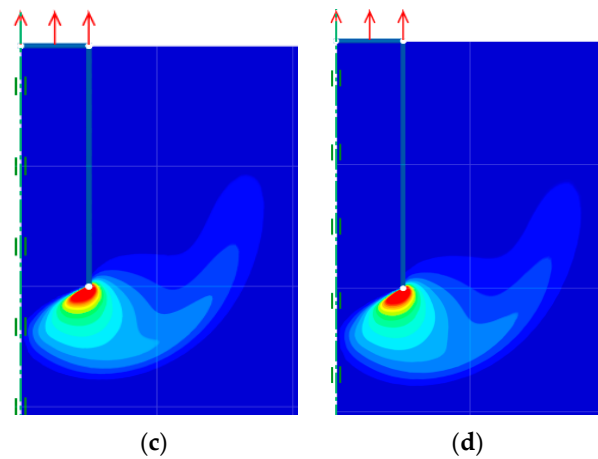


Figure 10. Comparison of shear dissipations of the cylindrical suction caissons for different values of α with $r_e = 0.7$, $L/D = 2$, $m = 2$: (a) $\alpha = 0$, (b) $\alpha = 0.4$, (c) $\alpha = 0.8$, (d) $\alpha = 1$.

The impact of the anisotropic undrained shear strength ratio r_e on the uplift capacity factor N is demonstrated in Figure 11 for the cases of $\alpha = 1$ and different values of m and L/D . Shown in Figure 11a–d are the cases of $L/D = (0.2, 0.6, 2, 10)$, respectively. The convex relationship between N and r_e is observed for all cases of m and L/D . The value of N increases with the rise of r_e due to the increase of the extension of the undrained shear strength. Additionally, the rate of the increase in N is developed when the value of m is growing. The influence of r_e on the failure patterns is examined for the cases of $r_e = (0.5, 0.7, 0.9, 1)$, as shown in Figure 12a–d, respectively. This investigation is based on the cases of $\alpha = 1$, $L/D = 5$, and $m = 5$. The results show that the size of the failure pattern is bigger in both horizontal and vertical directions when the value of r_e is greater.

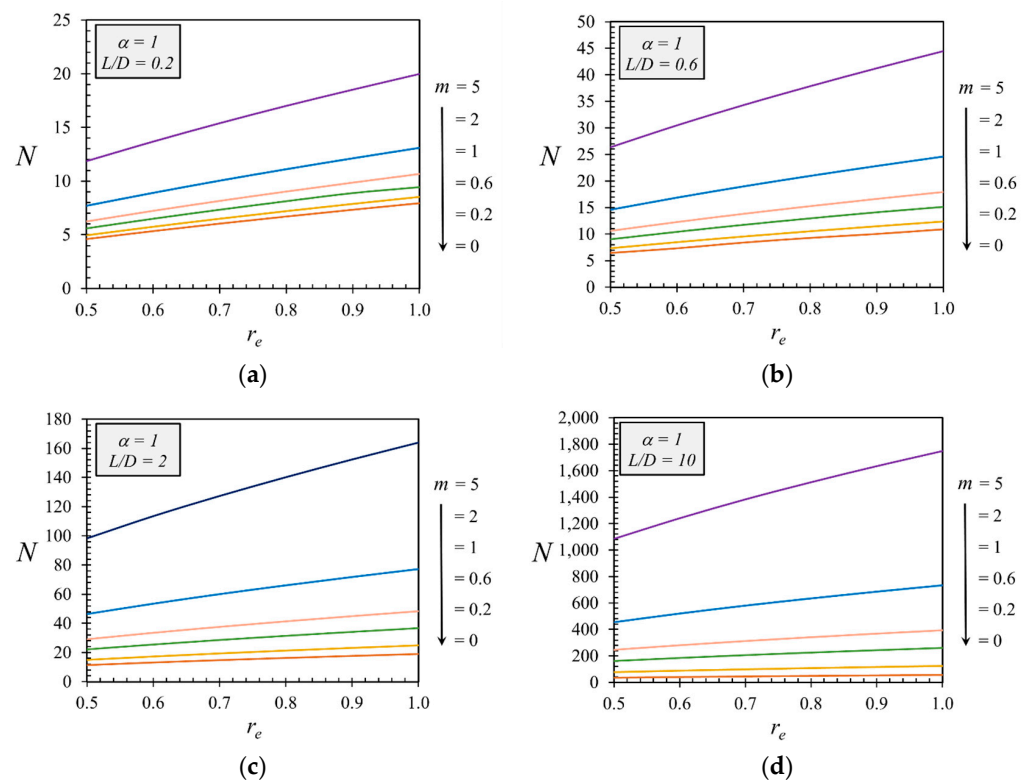


Figure 11. Impact of r_e on the uplift capacity factor N for the cases of $\alpha = 1$: (a) $L/D = 0.2$, (b) $L/D = 0.6$, (c) $L/D = 2$, (d) $L/D = 10$.

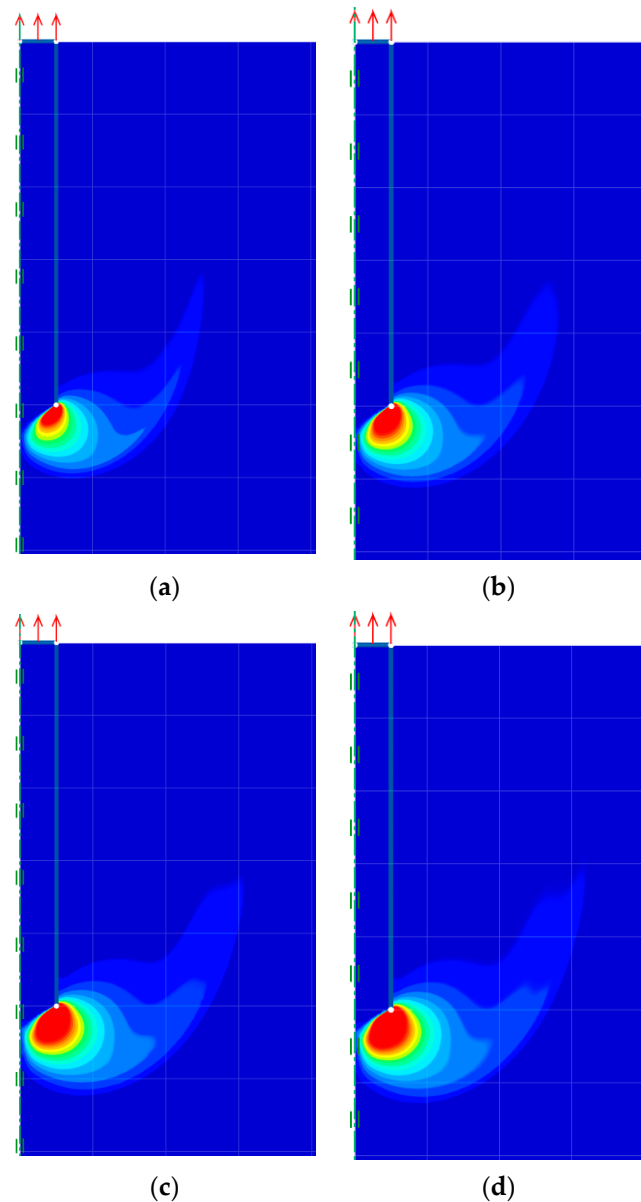


Figure 12. Comparison of shear dissipations of the cylindrical suction caissons for different values of r_e with $\alpha = 1$, $L/D = 5$, and $m = 5$: (a) $r_e = 0.5$, (b) $r_e = 0.7$, (c) $r_e = 0.9$, (d) $r_e = 1$.

6. Empirical Prediction by MARS Model

The above dimensionless parametric studies express that the coupling impacts among multiple input parameters are enormously complex. Thus, it is necessary to examine the sensitivity of each parameter on the uplift bearing factor of N . It is noted that the sensitivity analysis of all input parameters is useful for practical engineering because it can provide optimization strategies for the initial design of suction caissons. In this study, the multivariate adaptive regression splines (MARS) technique is applied in the sensitivity analysis.

MARS is a successful automated regression tool for fitting the relationship between input and out parameters in multi-dimensions. MARS is considered a curve-based machine learning model [47–50]. Compared to other machine learning approaches, such as artificial neurons networks, Gaussian process regression, stochastic gradient-boosting trees, and support vector regression, Mars seems to be more effective [47,48]. The concept of the MARS model is shown in Figure 13. MARS is partitioned data in many data groups that are suitable for the linear regression model. It aims to simplify a complex nonlinear regression

to a multi-linear regression. The boundary of each group is determined by Knot values. The position of the Knot is selected by an adaptive regression algorithm. The regression line in each data group is mathematically described by the basic function, as shown in Equation (7) [49,50].

$$\text{BF} = \max(0, x - t) = \begin{cases} x - t & \text{if } x \geq t \\ 0 & \text{otherwise} \end{cases} \quad (7)$$

where x is an input variable and t is a threshold value. The MARS algorithm includes two main steps. Firstly, MARS generates a number of basic functions, i.e., a number of data groups to increase the accuracy of the regression. Later, the least effective terms are cleared using a pruning algorithm based on generalized cross-validation (GCV) [51–53]. To build the closed-form equation between the input variables and output results, MARS combines basic functions, as follows:

$$f(x) = a_0 + \sum_{i=1}^M a_i g_i(X) \quad (8)$$

where a_0 is the constant, M is the number of BFs, g_i is the i th BF, and a_i is the coefficient of g_i . The details of the MARS model can be seen in Zhang [54].

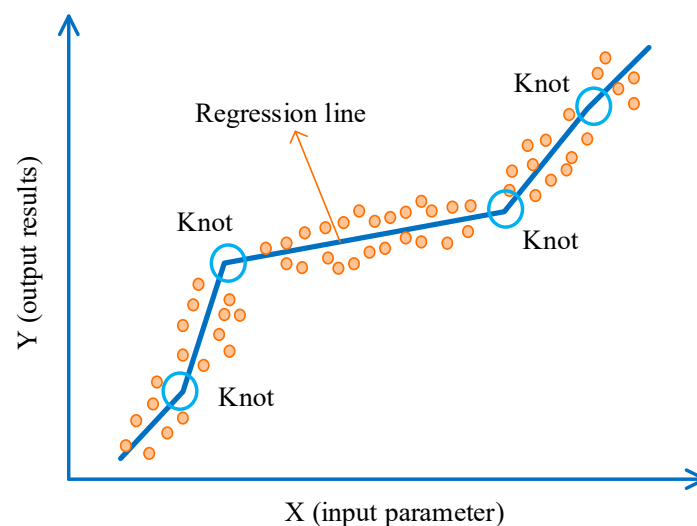


Figure 13. The MARS procedure.

Due to the effectiveness of the MARS model in data analysis, it was applied to various geotechnical issues. For instance, Lai et al. [55] adopted the MARS model to build the closed-form equation between six input parameters, and their corresponding output results in their analyses are the behavior of two adjacent open caissons. Furthermore, the impact of each parameter on their output results was also implemented. Zhang et al. [56] used MARS in the deep excavation problem to build the correlation equation between five input parameters and the lateral displacements of retaining walls in clays. Raja and Shukla [48] applied MARS in investigating the relationship between the settlement of the reinforcement of soil foundations and eight input parameters. By comparing MARS with four other machine learning methods, including extreme learning machines (ELM), Gaussian process regression (GPR), support vector regression (SVR), and stochastic gradient-boosting trees (SGBT), they suggested that MARS is a better model. In this study, with the multi-input parameters (four dimensionless input parameters) and the complex relationship between the input parameters and output uplift bearing factor N , the MARS model is a good approach to examine the influence of each input and output parameter.

The influence of each parameter can be described through the relative importance index in MARS. In this study, all 1296 output numerical results of the uplift bearing factor

N corresponding to the input values of dimensionless parameters (i.e., L/D , r_e , α , m), which are shown in Tables 2–4, are used to access their sensitivities using Mars. Figure 14 demonstrates the relative importance index for all considered dimensionless parameters. It can be seen that the relative importance index of L/D is 100%, while those parameters such as m , α , and r_e are 90.54%, 37.08%, and 20.81%, respectively. Note that the value of 100% in the relative importance index expresses that the L/D parameter is the most important input parameter that has the largest impact on the output value of the uplift bearing factor N . A smaller value of the relative importance index corresponds to a lesser effect of each parameter on N .

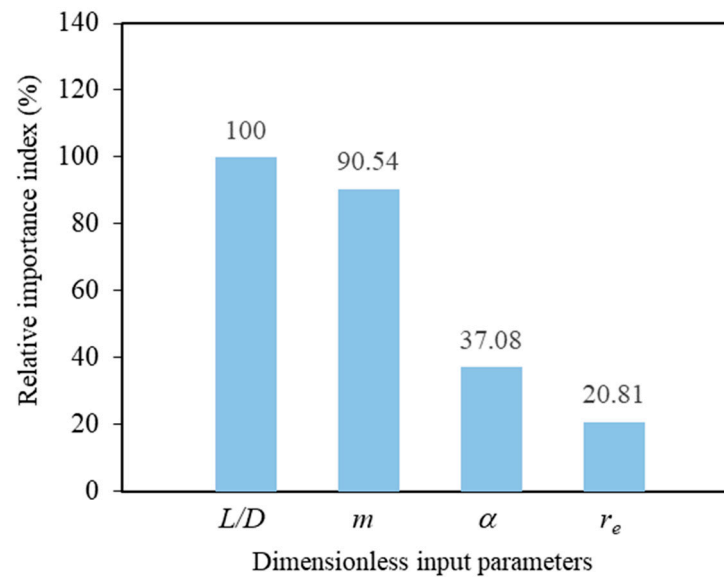


Figure 14. Relative importance index for each dimensionless parameter.

Given the high impacts of the input dimensionless parameters, it is useful to propose a more efficient tool such as an empirical design equation that can be easily used to predict the uplift stability factor of a suction caisson in anisotropic and non-homogenous clay. The multivariate adaptive regression splines (MARS) model is also employed to develop the empirical equation. The MARS algorithm does not need specific assumptions to show the correlation relationships between input and output parameters. The optimal equation $f(x)$ with the smallest GCV value after a pruning algorithm is proposed based on a linear combination of BFs, as shown in Equation (8).

Note that the set of 1296 numerical results shown in Tables 2–4 is also used as the training data to propose the empirical design equation. The list of basic functions (BFs) and the optimal empirical equation to predict the uplift bearing factor N are shown in Table 5. The comparison between the predicted values of N from the optimal empirical equation and those from FELA is shown in Figure 15. It can be seen that a high accuracy of the optimal empirical equation is obtained, where the coefficient of determination (R^2) is very high (about 100%). Note that the use of many basic functions (BFs) can provide more accurate results. Thus, there are 60 BFs in the design equation in which these functions can be easily used by engineering practitioners by inputting them into the user-defined function in Excel Marco.

Table 5. Basic functions (BF) and mathematical equations in MARS model for uplift bearing factor N .

BF	Equation	BF	Equation	BF	Equation
BF1	$=\max(0, L/D - 5)$;	BF19	$=\max(0, L/D - 2) \times BF17$;	BF39	$=\max(0, 2 - L/D) \times BF13$;
BF2	$=\max(0, 5 - L/D)$;	BF20	$=\max(0, 2 - vL/D) \times BF17$;	BF40	$=\max(0, L/D - 2) \times BF37$;
BF3	$=\max(0, m - 0) \times BF1$;	BF21	$=\max(0, r_e - 0.6) \times BF4$;	BF41	$=\max(0, 2 - L/D) \times BF37$;
BF4	$=\max(0, \alpha + 5.96046 \times 10^{-8}) \times BF3$;	BF22	$=\max(0, 0.6 - r_e) \times BF4$;	BF42	$=\max(0, L/D - 0.6) \times BF37$;
BF5	$=\max(0, m - 0)$;	BF23	$=\max(0, \alpha - 0.6) \times BF5$;	BF44	$=\max(0, \alpha - 0.8) \times BF33$;
BF6	$=\max(0, L/D - 2) \times BF5$;	BF24	$=\max(0, 0.6 - \alpha) \times BF5$;	BF45	$=\max(0, 0.8 - \alpha) \times BF33$;
BF7	$=\max(0, 2 - L/D) \times BF5$;	BF25	$=\max(0, L/D - 2) \times BF24$;	BF46	$=\max(0, r_e - 0.9) \times BF10$;
BF8	$=\max(0, r_e - 0.7) \times BF6$;	BF26	$=\max(0, 2 - L/D) \times BF24$;	BF48	$=\max(0, \alpha - 0.2) \times BF13$;
BF9	$=\max(0, 0.7 - r_e) \times BF6$;	BF27	$=\max(0, r_e - 0.7) \times BF15$;	BF49	$=\max(0, 0.2 - \alpha) \times BF13$;
BF10	$=\max(0, \alpha + 5.96046 \times 10^{-8}) \times BF6$;	BF28	$=\max(0, 0.7 - r_e) \times BF15$;	BF50	$=\max(0, \alpha - 0.8) \times BF9$;
BF11	$=\max(0, r_e - 0.8) \times BF10$;	BF29	$=\max(0, L/D - 1) \times BF23$;	BF51	$=\max(0, 0.8 - \alpha) \times BF9$;
BF12	$=\max(0, 0.8 - r_e) \times BF10$;	BF30	$=\max(0, 1 - L/D) \times BF23$;	BF52	$=\max(0, m - 0.6)$;
BF13	$=\max(0, r_e - 0.5)$;	BF31	$=\max(0, L/D - 5) \times BF18$;	BF55	$=\max(0, 0.6 - L/D) \times BF52$;
BF14	$=\max(0, \alpha + 5.96046 \times 10^{-8})$;	BF32	$=\max(0, 5 - L/D) \times BF18$;	BF57	$=\max(0, 0.9 - r_e) \times BF33$;
BF15	$=\max(0, L/D - 2) \times BF14$;	BF33	$=\max(0, L/D - 1) \times BF5$;	BF58	$=\max(0, \alpha - 0.2) \times BF57$;
BF16	$=\max(0, 2 - L/D) \times BF14$;	BF35	$=\max(0, L/D - 5) \times BF17$;	BF59	$=\max(0, 0.2 - \alpha) \times BF57$;
BF17	$=\max(0, r_e - 0.6) \times BF5$;	BF37	$=\max(0, \alpha + 5.96046 \times 10^{-8}) \times BF17$;	BF60	$=\max(0, \alpha + 5.96046 \times 10^{-8}) \times BF39$;
BF18	$=\max(0, 0.6 - r_e) \times BF5$;	BF38	$=\max(0, L/D - 2) \times BF13$;		

$$N = 7.34338 + 0.260828 \times BF1 - 0.586461 \times BF2 + 1.55056 \times BF3 + 11.9728 \times BF4 + 16.2314 \times BF5 + 9.13961 \times BF6 - 8.05533 \times BF7 - 0.983972 \times BF8 - 1.13233 \times BF9 + 8.1486 \times BF10 + 6.52061 \times BF11 - 8.4729 \times BF12 + 11.2154 \times BF13 + 6.17607 \times BF14 + 3.28002 \times BF15 - 3.2612 \times BF16 + 14.6437 \times BF17 - 52.8027 \times BF18 + 11.351 \times BF19 - 7.22317 \times BF20 + 10.0719 \times BF21 - 12.5708 \times BF22 + 1.71651 \times BF23 - 4.13455 \times BF24 - 2.20414 \times BF25 + 2.23358 \times BF26 + 2.29874 \times BF27 - 3.668 \times BF28 + 2.0948 \times BF29 - 2.13364 \times BF30 - 13.8382 \times BF31 + 10.4966 \times BF32 + 3.28344 \times BF33 + 2.3659 \times BF35 + 1.94912 \times BF37 + 0.48867 \times BF38 - 2.67278 \times BF39 - 3.96712 \times BF40 - 0.989502 \times BF41 + 2.07672 \times BF42 + 3.32143 \times BF44 - 3.44554 \times BF45 + 2.48173 \times BF46 + 4.8134 \times BF48 - 6.4998 \times BF49 - 3.70576 \times BF50 + 1.68277 \times BF51 - 0.617768 \times BF52 + 1.17368 \times BF55 - 1.14761 \times BF57 - 3.32378 \times BF58 + 3.09802 \times BF59 - 1.67664 \times BF60.$$

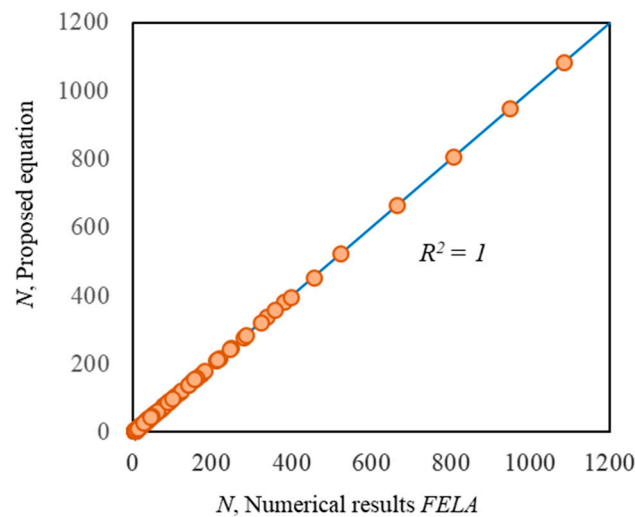


Figure 15. Comparison N from the proposed equation and FELA results.

7. Limitation

The LB and UB FELA are used to determine the uplift capacity factor of a suction caisson in anisotropic and inhomogeneous clay under axisymmetric conditions. Although this is the first time that the influences of the anisotropic behaviors of clay are carefully investigated, it is restricted by certain assumptions and should be investigated further as follows:

1. All of the computed design charts are restricted with the assumption of undrained soil conditions, which cannot be used in drained soil conditions;
2. The proposed equation for the uplift capacity factor of a suction caisson in anisotropic and inhomogeneous clay is suitable for the ranges of dimensionless input parameters, as presented earlier in Table 1. The results may not be accurate if the input values are out of these ranges;
3. The present solutions cannot be used for cases of multi-layered soils;
4. If there are two caissons nearby, the effect of the spacing between these two caissons should be further analyzed by adopting a three-dimensional FELA approach;
5. Code/guidelines or recommendations for designing the steel or concrete walls of cylindrical caissons or cylindrical systems should be carried out as future works. Examples of similar guidance for designing steel tanks can be found in references [57,58].

8. Conclusions

This paper investigates the uplift resistance of suction caisson foundations in anisotropic and inhomogeneous clays. Through verification with results from the literature, the numerical results of the proposed works are well fitted with the previous solutions. The parameters considered in this study are m (ratio of inhomogeneity), α (adhesion factor), L/D (ratio of depth over diameter), and r_e (ratio of anisotropic undrained shear strengths), which have a strong influence on the uplift resistance of suction caisson foundations. The results show that the uplift resistance is a nonlinear increase with L/D and r_e and a linear increase with m and α in all investigated cases. The influence of these investigated parameters (m , α , L/D , and r_e) on the failure mechanisms is also determined. The size of the failure zone increases as L/D and m increase, and there are minor changes as α and r_e increase.

By comparing the sensitivity of each parameter on the uplift resistance factor by employing the MARS model, the ratio of depth over diameter (L/D) is the most important one for the ratio of inhomogeneity (m), the adhesion factor (α) and the ratio of anisotropic undrained shear strengths (r_e), respectively. Based on the MARS model, the efficient empirical design equation is then proposed with a very accurate prediction for all FELA results.

Author Contributions: Conceptualization, T.J., V.Q.L. and S.K.; methodology, T.J., V.Q.L. and S.K.; software, T.J., V.Q.L., S.K., T.S.N., C.N.V., C.T. and P.N.; validation, T.J., V.Q.L., S.K., T.S.N., C.N.V., C.T. and P.N.; formal analysis, T.J., V.Q.L., S.K., T.S.N., C.N.V., C.T. and P.N.; investigation, T.J., V.Q.L., S.K., T.S.N., C.N.V., C.T. and P.N.; resources, T.J., V.Q.L. and S.K.; data curation, T.J., V.Q.L., S.K., T.S.N., C.N.V., C.T. and P.N.; writing—original draft preparation, T.J., V.Q.L. and S.K.; writing—review and editing, T.J., V.Q.L. and S.K.; visualization, T.J., V.Q.L., S.K., T.S.N., C.N.V., C.T. and P.N.; supervision, T.J., V.Q.L. and S.K.; project administration, T.J., V.Q.L. and S.K.; funding acquisition, T.J., V.Q.L. and S.K. All authors have read and agreed to the published version of the manuscript.

Funding: This research was supported by the Structural and Foundation Engineering Research Unit, Thammasat University.

Institutional Review Board Statement: Not applicable.

Informed Consent Statement: Not applicable.

Data Availability Statement: The data and materials in this paper are available.

Acknowledgments: We would like to thank Ho Chi Minh City University of Technology (HCMUT), VNU-HCM for the support of time and facilities for this study.

Conflicts of Interest: The authors declare no conflict of interest.

References

1. Mortlock, T.R.; Goodwin, I.D.; Turner, I.L. Nearshore SWAN model sensitivities to measured and modelled offshore wave scenarios at an embayed beach compartment, NSW, Australia. *Aust. J. Civ. Eng.* **2014**, *12*, 67–82. [[CrossRef](#)]
2. Mahmoodian, M. Structural reliability assessment of corroded offshore pipelines. *Aust. J. Civ. Eng.* **2020**. [[CrossRef](#)]
3. Randolph, M.; Gourvence, S. *Offshore Geotechnical Engineering*; Spon Press Taylor & Francis: Abingdon, UK, 2011.

4. Andersen, K.H.; Dyvik, R.; Schroder, K.; Hansteen, O.E.; Bysveen, S. Field test of anchors in clay II: Predictions and interpretation. *J. Geotech. Geoenviron. Eng.* **1993**, *119*, 1532–1549. [[CrossRef](#)]
5. Dyvik, R.; Andersen, K.H.; Hansen, S.B.; Christophersen, H.P. Field test of anchors in clay I: Description. *J. Geotech. Geoenviron. Eng.* **1993**, *119*, 1515–1531. [[CrossRef](#)]
6. Clukey, E.C.; Morrison, M.J. A Centrifuge and analytical study to evaluate suction caissons for TLP applications in gulf of Mexico. In *Design and Performance of Deep Foundation*; American Society of Civil Engineers: Reston, VA, USA, 1993; pp. 141–156.
7. Cauble, D.F. Experimental Measurements for a Model Suction Caisson. Ph.D. Thesis, Massachusetts Institute of Technology, Cambridge, MA, USA, 1996.
8. Geer, M. Analysis of Pile and Suction Caisson Behavior in Axial Loading. Ph.D. Thesis, Massachusetts Institute of Technology, Cambridge, MA, USA, 1996.
9. Bransby, M.F.; Yun, G. The undrained capacity of skirted strip foundations under combined loading. *Géotechnique* **2009**, *59*, 115–125. [[CrossRef](#)]
10. Gourvenec, S. Effect of embedment on the undrained capacity of shallow foundations under general loading. *Géotechnique* **2008**, *58*, 177–185. [[CrossRef](#)]
11. Gourvenec, S.; Barnett, S. Undrained failure envelope for skirted foundations under general loading. *Géotechnique* **2011**, *61*, 263–270. [[CrossRef](#)]
12. Yun, G.; Bransby, M.F. The undrained vertical bearing capacity of skirted foundations. *Soils Found.* **2007**, *47*, 493–505. [[CrossRef](#)]
13. Mana, D.S.K.; Gourvenec, S.; Martin, C.M. Critical skirt spacing for shallow foundations under general loading. *J. Geotech. Geoenviron. Eng.* **2013**, *139*, 1554–1566. [[CrossRef](#)]
14. Jin, Z.; Yin, Z.Y.; Kotronis, P.; Ji, Y.F. Numerical investigation on evolving failure of caisson foundation in sand using the combined Lagrangian-SPH method. *Mar. Georesources Geotechnol.* **2019**, *37*, 23–35. [[CrossRef](#)]
15. Liu, J.; Chen, X.; Zhu, Z.; Wang, B.; Liu, F.; Xu, J.; Zhang, M. Investigation of scour effects on lateral behaviors of suction caisson. *Mar. Georesources Geotechnol.* **2019**, *37*, 142–151. [[CrossRef](#)]
16. Ukritchon, B.; Wongtoythong, P.; Keawsawasvong, S. New design equation for undrained uplift capacity of suction caissons considering combined effects of caisson aspect ratio, adhesion factor at interface, and linearly increasing strength. *Appl. Ocean. Res.* **2018**, *75*, 1–14. [[CrossRef](#)]
17. Keawsawasvong, S.; Ukritchon, B. Finite element limit analysis of uplift capacity of planar caissons in clay. *Comput. Geotech.* **2016**, *75*, 12–17. [[CrossRef](#)]
18. Ukritchon, B.; Keawsawasvong, S. Undrained uplift capacity of cylindrical suction caissons by finite element limit analysis. *Comput. Geotech.* **2016**, *80*, 301–311. [[CrossRef](#)]
19. Sloan, S.W. Geotechnical stability analysis. *Géotechnique* **2013**, *63*, 531–572. [[CrossRef](#)]
20. Ladd, C.C. Stability evaluations during stage construction. *J. Geotech. Eng.* **1991**, *117*, 540–615. [[CrossRef](#)]
21. Ladd, C.C.; DeGroot, D.J. Recommended practice for soft ground site characterization. Arthur Casagrande Lecture. In Proceedings of the 12th Panamerican Conference on Soil Mechanics and Geotechnical Engineering, Cambridge, UK, 22–26 June 2003.
22. Krabbenhoft, K.; Lyamin, A.V. Generalised Tresca criterion for undrained total stress analysis. *Geotech. Lett.* **2015**, *5*, 313–317. [[CrossRef](#)]
23. Krabbenhoft, K.; Galindo-Torres, S.A.; Zhang, X.; Krabbenhoft, J. AUS: Anisotropic undrained shear strength model for clays. *Int. J. Numer. Anal. Methods Geomech.* **2019**, *43*, 2652–2666. [[CrossRef](#)]
24. Ukritchon, B.; Keawsawasvong, S. Lower bound limit analysis of an anisotropic undrained strength criterion using second-order cone programming. *Int. J. Numer. Anal. Methods Geomech.* **2018**, *42*, 1016–1033. [[CrossRef](#)]
25. Ukritchon, B.; Keawsawasvong, S. Lower bound solutions for undrained face stability of plane strain tunnel headings in anisotropic and non-homogeneous clays. *Comput. Geotech.* **2019**, *112*, 204–217. [[CrossRef](#)]
26. Ukritchon, B.; Keawsawasvong, S. Three-dimensional lower bound finite element limit analysis of an anisotropic undrained strength criterion using second-order cone programming. *Comput. Geotech.* **2019**, *106*, 327–344. [[CrossRef](#)]
27. Ukritchon, B.; Keawsawasvong, S. Undrained lower bound solutions for end bearing capacity of shallow cylindrical piles in non-homogeneous and anisotropic clay. *Int. J. Numer. Anal. Methods Geomech.* **2020**, *44*, 596–632. [[CrossRef](#)]
28. Ukritchon, B.; Keawsawasvong, S. Undrained stability of unlined square tunnels in clays with linearly increasing anisotropic shear strength. *Geotech. Geol. Eng.* **2020**, *38*, 897–915. [[CrossRef](#)]
29. Keawsawasvong, S.; Ukritchon, B. Undrained stability of plane strain active trapdoors in anisotropic and non-homogeneous clays. *Tunn. Undergr. Space Technol.* **2021**, *107*, 103628. [[CrossRef](#)]
30. Keawsawasvong, S.; Ukritchon, B. Design equation for stability of a cylindrical tunnel in an anisotropic and heterogeneous clay. *Undergr. Space* **2021**, in press.
31. Yodsomjai, W.; Keawsawasvong, S.; Senjuntichai, T. Undrained stability of unsupported conical slopes in anisotropic clays based on AUS failure criterion. *Transp. Infrastruct. Geotechnol.* **2021**, *8*, 557–568. [[CrossRef](#)]
32. Keawsawasvong, S.; Lawongkerd, J. Influences of anisotropic undrained shear strengths of clays on pullout capacity of planar caissons. *Sci. Technol. Asia* **2021**, *26*, 90–98.
33. Nguyen, D.K.; Nguyen, T.P.; Keawsawasvong, S.; Lai, V.Q. Vertical uplift capacity of circular anchors in clay by considering anisotropy and non-homogeneity. *Transp. Infrastruct. Geotechnol.* **2021**, in press. [[CrossRef](#)]

34. Keawsawasvong, S.; Yoonirundorn, K.; Senjuntichai, T. Uplift capacity factor for cylindrical suction caissons in anisotropic clays based on Anisotropic Undrained Shear failure criterion. *Transp. Infrastruct. Geotechnol.* **2021**, *8*, 629–644. [[CrossRef](#)]
35. Keawsawasvong, S.; Shiau, J.; Ngamkhanong, C.; Lai, V.Q.; Thongchom, C. Undrained Stability of Ring Foundations: Axisymmetry, Anisotropy, and Nonhomogeneity. *Int. J. Geomech.* **2022**, *22*, 04021253. [[CrossRef](#)]
36. Lai, V.Q.; Nguyen, D.K.; Banyong, R.; Keawsawasvong, S. Limit analysis solutions for stability factor of unsupported conical slopes in clays with heterogeneity and anisotropy. *Int. J. Comput. Mater. Sci. Eng.* **2022**, *11*, 2150030–2150128. [[CrossRef](#)]
37. Lai, V.Q.; Banyong, R.; Keawsawasvong, S. Stability of limiting pressure behind soil gaps in contiguous pile walls in anisotropic clays. *Eng. Fail. Anal.* **2022**, *134*, 106049. [[CrossRef](#)]
38. Housley, G.T.; Martin, C.M. Undrained bearing capacity factors for conical footings on clay. *Géotechnique* **2003**, *53*, 513–520. [[CrossRef](#)]
39. Keawsawasvong, S. Bearing capacity of conical footings on clays considering combined effects of anisotropy and non-homogeneity. *Ships Offshore Struct.* 2021, in press. [[CrossRef](#)]
40. Bishop, A.W. The strength of soils as engineering materials. *Géotechnique* **1966**, *16*, 89–128. [[CrossRef](#)]
41. Oteuil, A.; Oralbek, A.; Mukhamet, T.; Moon, S.W.; Kim, J.; Tokbolat, S.; Satyanaga, A. Robust Analysis and Design of Bored Pile Considering Uncertain Parameters. *Indian Geotech. J.* 2022, in press. [[CrossRef](#)]
42. Zhanabayeva, A.; Sagidullina, N.; Kim, J.; Satyanaga, A.; Lee, D.; Moon, S.W. Comparative Analysis of Kazakhstani and European Design Specifications: Raft Foundation, Pile Foundation, and Piled Raft Foundation. *Appl. Sci.* **2021**, *11*, 3099. [[CrossRef](#)]
43. Krabbenhoft, K.; Lyamin, A.; Krabbenhoft, J. Optum Computational Engineering (OptumG2). 2015. Available online: www.optumce.com (accessed on 2 March 2022).
44. Ukritchon, B.; Keawsawasvong, S. Error in Ito and Matsui's limit equilibrium solution of lateral force on a row of stabilizing piles. *J. Geotech. Geoenviron. Eng.* **2017**, *143*, 02817004. [[CrossRef](#)]
45. Ukritchon, B.; Yoang, S.; Keawsawasvong, S. Undrained stability of unsupported rectangular excavations in non-homogeneous clays. *Comput. Geotech.* **2020**, *117*, 103281. [[CrossRef](#)]
46. Keawsawasvong, S.; Lai, V.Q. End bearing capacity factor for annular foundations embedded in clay considering the effect of the adhesion factor. *Int. J. Geosynth. Ground Eng.* **2021**, *7*, 1–10. [[CrossRef](#)]
47. Wu, L.; Fan, J. Comparison of neuron-based, kernel-based, tree-based and curve-based machine learning models for predicting daily reference evapotranspiration. *PLoS ONE* **2019**, *14*, e0217520. [[CrossRef](#)]
48. Raja, M.N.A.; Shukla, S.K. Multivariate adaptive regression splines model for reinforced soil foundations. *Geosynth. Int.* **2021**, *28*, 368–390. [[CrossRef](#)]
49. Sirimontree, S.; Jearsiripongkul, T.; Lai, V.Q.; Eskandarinejad, A.; Lawongkerd, J.; Seehavong, S.; Thongchom, C.; Nuaklong, P.; Keawsawasvong, S. Prediction of Penetration Resistance of a Spherical Penetrometer in Clay Using Multivariate Adaptive Regression Splines Model. *Sustainability* **2022**, *14*, 3222. [[CrossRef](#)]
50. Lai, V.Q.; Shiau, J.; Keawsawasvong, D.T. Bearing Capacity of Ring Foundations on Anisotropic and Heterogeneous Clays ~ FEA, NGI-ADP, and MARS. *Geotech. Geol. Eng.* 2022; accepted.
51. Friedman, J.H. Multivariate adaptive regression splines. *Ann. Stat.* **1991**, *19*, 1–67. [[CrossRef](#)]
52. Caraka, R.E.; Chen, R.C.; Bakar, S.A.; Tahmid, M.; Toharudin, T.; Pardamean, B. Employing Best Input SVR Robust Lost Function with Nature-Inspired Metaheuristics in Wind Speed Energy Forecasting. *IAENG Int. J. Comput. Sci.* **2020**, *47*, 572–584.
53. Stoklosa, J.; Warton, D.I. A Generalized Estimating Equation Approach to Multivariate Adaptive Regression Splines. *J. Comput. Graph. Stat.* **2018**, *27*, 245–253. [[CrossRef](#)]
54. Zhang, W. *MARS Applications in Geotechnical Engineering Systems*; Springer: Singapore, 2020.
55. Lai, F.; Zhang, N.; Liu, S.; Sun, Y.; Li, Y. Ground movements induced by installation of twin large diameter deeply-buried caissons: 3D numerical modeling. *Acta Geotech.* **2021**, *16*, 2933–2961. [[CrossRef](#)]
56. Zhang, W.; Zhang, R.; Goh, A.T.C. MARS inverse analysis of soil and wall properties for braced excavations in clays. *Geomech. Eng.* **2018**, *16*, 577–588.
57. González, E.; Almazán, J.; Beltrán, J.; Herrera, R.; Sandoval, V. Performance of stainless steel winery tanks during the 02/27/2010 Maule Earthquake. *Eng. Struct.* **2013**, *56*, 1402–1418. [[CrossRef](#)]
58. Brunesi, E.; Nascimbene, R.; Pagani, M.; Beilic, D. Seismic performance of storage steel tanks during the May 2012 Emilia, Italy, Earthquakes. *J. Perform. Constr. Facil.* **2015**, *29*, 04014137. [[CrossRef](#)]